We wish to thank both referees and all those who provided comments for this manuscript for their thorough reading of the manuscript and useful comments. We addressed all points raised as follows:

Anonymous Referee #1

The paper contains interesting and useful results from two experiments reproducing stratified flows: one with heat forcing and one with concentration forcing. Spectra are discussed and spectral law evidenced.
The second experiment using a fresh water source could be better introduced in section 2. It is not clear if a steady state is sought for or if the whole experiment is transient.
page 1511 - para 25 imager should be image ?
Response: No, the imager is the sensor of the video camera.

page 1514 - para 10 There is a typo in Rayleigh
Response: Corrected

page 1518 - para 10 'The values of KR are marked ...' I think what is meant is 'The location of KR' ?
Response: Corrected

In Figure 5 it could be useful to indicate Kf
Response: Done

page 1520 - para 20
'..., the instability as a source of ...' there seems to be a verb missing in the sentence.
Response: Corrected

W.-G. Fruh (Referee #2)

Overall, the paper presents new, interesting and useful experiments and results. Some aspects of the experimental set-up and method are not as clear as they could be. The approach taken for the spectral analysis and some of the key results should be discussed more.

Questions or suggestions to the authors
Thermal forcing
1. Thermal forcing: I found it difficult to interpret the results in Figure 3 without knowing the shape and size of the heating elements. It would help to describe the heating wires in a bit more detail in the experimental technique section (and show a top view of the tank to show the wires). My initial thought was that it would be a spiral of a resistive wire, from the centre to the perimeter but looking at the results it appears to be a set of parallel wires. What is the spacing of the wire? Are the wires on top of the bottom surface as Figure 1 suggests, or are they embedded in the base – if so, how deep? As that

would expect how strongly localized the heat source is to the line of the wire or slightly broadened through the heat conduction through the base.

Response: Following the suggestion of the referee we described the shape of the heating wire and included a figure (Fig. 1 b) which shows the wire pattern and the view of the flow in the beginning of the experiment.

2. Thermal forcing and experimental time: I presume the clock starts counting after the (initially stagnant and isothermal) fluid has reached solid-body rotation, and at the instant when the heating is switched on. Is that right? Is the heat dissipation from the wires maintained at a constant level throughout the duration of the experiment?

Response: Yes, the clock starts when the heating is switched on. It is the constant heat flux setup and the system was not thermally insulated. At certain point in time (after about 45 min) a balance between heat supply and heat loss was achieved.

Saline forcing

3. Salinity: Can you explain the procedure in a bit more detail? If I understand it correctly, the forcing is more through the baroclinicity caused by the density difference between the salt and fresh water, rather than by salinity gradients. Is that right? If so, what is the temperature difference (or the corresponding BruntVaissala frequency / Froude number)? Also, the instability will depend on the depths of the two layers. Can you quantify that?

Response: Yes, the forcing is due to internal dynamics of the stratified sheared flow, the baroclinicity. The salinity difference is 30 ppm. The instability can theoretically be dependent on the depth ratio of the layers. The depth of the upper (fresh) layer varies with radial distance though, so it is far from an idealized constant depth setup. Also, the perturbations seem to be correlated in the radial direction that is perhaps more dynamically significant than a possible dependence on the depth ratio.

4. Fundamental mechanism: If I understood the previous item correctly, I presume that the forcing mechanism is through baroclinic instability rather than direct forcing, since you are setting up a stably-stratified two-layer system. Is that right?

Response: Yes, please see our comment above.

5. Implementation: How do the fresh-water addition and the experimental observation actually relate? It seems from some late comments, that the experiment time starts at the end of the water addition. Is that correct? If so, could you explain what actually happens during the fresh water addition and after? And, would then seem that the experiment would go through a cycle of baroclinic instability (caused by the velocities set up during the water addition), growth of 'baroclinic waves', followed by decay of these waves through friction and possibly other instabilities (e.g. wave breaking / frontal barotropic instability / vertical mixing of fresh-salt water). If so, what are the typical life-spans of the various stages, or the total cycle? As you can see, I struggle to understand and interpret your saline forcing experiment and its results and would welcome more explanation.

Response: We expanded the description of the flow dynamics in Sec. 3.1 to clarify the points raised by the referee.

Spectral Analysis
I am not entirely sure on the area over which you carry out the spectral analysis, and how valid your assertion is that the Cartesian FFT-based spectral analysis is sufficiently accurately in the cylindrical domain is not entirely clear without getting a bit more information.

6. Can you explain and discuss the domain for the spectral analysis a bit better, and what effects turning the cylindrical coordinates into a local Cartesian has? Did I understand it correctly that you are using an annular domain with an inner radius of 8 cm and an outer radius of 42 cm? It might be helpful to show an illustration of the tank and of the analysis domain (with a highly reduced set of points for the 'Cartesian' grid); maybe something like

Response: We chose not to include an additional figure in this relatively short paper because the coordinate system is described in the beginning of Sec.3.2 and it is one widely used in oceanography. For the discussion of issues of the wide-gap geometry please also see our response to #8.

7. If the coordinate system is Cartesian centred at r0 = 25 cm, then the distance between two adjacent points on the inner-most ring is made equal to that at the outermost ring. With a radius ratio or 8cm/42cm = 0.19, or a width-to-mean radius of curvature of 34cm/25cm = 1.36, your analysis domain is definitely a 'wide-gap' geometry, where the changes in local curvature would be expected to be fairly large.

Response: Please see our response to #8.

8. Presumably the wave numbers are equally stretched/compressed at radii different from r0 ? What does that mean for 'equating' kx at r = 8 cm (or y= – 17cm) with the same kx at r= 42 cm (or y = + 17 cm)? Would you not expect that small-scale turbulence (of length scale << 2πr) should not be expected to be effected much by the curvature (and hence a true size of a certain size is dynamically similar to features of the same size but at a different radius)? At the other end of the scale, for features approaching the 'length' of the channel, eg. 2πr/N, where N is smaller than, say 5, the 'available' space affects the feature. Would we not expect the wave number N to be more important than the local length scale – and the stretching of the tangential component is valid? Do you think it might be worth generating contour plots of spectral amplitude of in the tangential direction (ie, plot contours of E(kx, y) against kx and y) ?

Response: Yes, indeed, there is an issue of kx wavenumbers being quite different along the inner and outer rings. This results in spectra being somewhat diffused along kx-axis. An advantage of the wide cap is, of course, better resolution of smaller ky wavenumbers. Thus, it is a trade-off. We have also calculated the spectra for a narrow gap of only 3 cm half-width (not shown here). The spectra are somewhat more concentrated in kx-direction but the resolution in the ky is lost. Perhaps, the better thing to do here is to do the Fourier-Bessel decomposition. We are working on this and will report the results elsewhere. We followed the suggestion of the referee and plotted spectra E(kx) measured along three circles of radius r = 8, 25 and 42 cm (see below). The spectra look similar to each other. We did not show this figure in the paper as it only serves as a diagnostic.

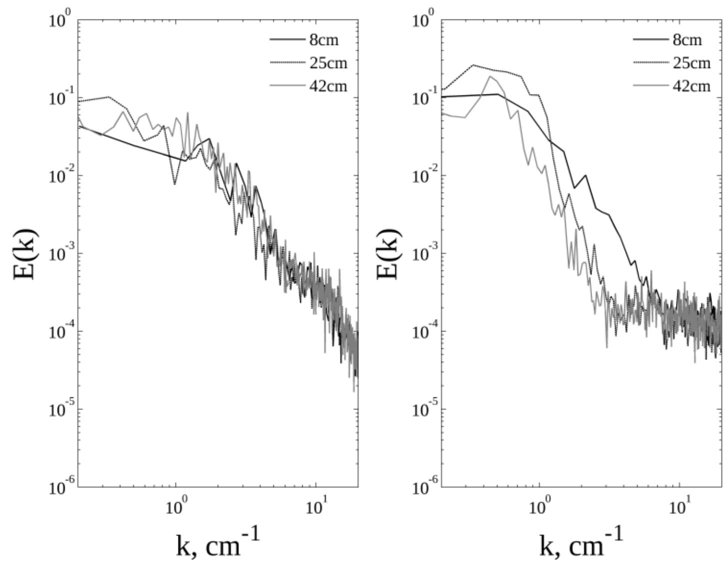

9. By the way, the circles and figure-of-eight in Figure 4 are virtually invisible. Is there any way you can make them more prominent?

Response: Done

10. For the discussion of the 1D spectra in Figure 5, it would be helpful to indicate the location (e.g. by a vertical line) of the forcing length scale (spacing of the heating wires 1.4 cm–1 and/or of the thermal forcing length scale 2.5 cm–1 ; the radius of deformation 1.2 cm–1 and the most unstable wave number 0.77 cm–1) and the Rhines scale of 0.45 cm–1

Response: Done

11. Any ideas what determines the length scale of the thermal forcing?

Response: Yes, it is Rd that determines the scale of eddies. Please see discussion in the beginning of Sec 3.1.

12. How do you achieve a spectral range for the 1D wave number of substantially larger than 10 cm–1 with your spatial resolution of 0.2cm x 0.2cm (as you stated earlier)?

Response: there is a factor of 2π there.

13. Page 1520, line 1: 'The steeper slope in the second experiment is due to the particular nature of this two-layer baroclinic flow.' Can you explain or interpret this a bit more?

Response: We believe that the steeper slope is due to the baroclinic nature of this flow (in contrast to barotropic and, therefore, almost 2D flow in the thermal experiment). We modified this discussion to make it clearer.

14. Not everybody might be familiar with the Sobel gradient operators (p.1512, line21). Could you provide a reference?

Response: Done

Typographical points Convention used: ; delete ; {comments}

• p.1508, line 5: top of saline layer • line 16: β-effect …
• line 17: spectra in the wavenumber space {either: become} of a {or: form} a figure eight {It is more commonly referred to as 'figure-of-eight' rather than just 'figure eight'}
• p.1511, line 7: surface of rotating
• line 10: obtain velocity
• line 18: It , however is perfectly
• line 20: paraboloidal … used as a mirror of the Newtonian
• p.1512, line 3: barotropic
• p.1513, line 1-2: Note that in a stratified fluid (as … forcing) velocity.. is, in fact , a barotropic …
• line 6: 2015) and is
• p. 1514, line 12: Rayleigh {missing i}
• p. 1515, line 9: water, an
• line 10: Thus, two-layer
• p.1517, line 2: two-dimensional…
• p.1518, line 21: resembles figure eight
• p.1519, line 2: that turbulent
• line 5: instead (linear)
• line 6: towards k_y
• line 28: presence of – 3 slope
• p.1520, line 1: steeper…
• line 5-6: {This is a bit ambiguous as to whether 'both' refers to the two references cited in the previous sentence or to your two experiments. It would be much clearer to refer to your experiments if you simply started a new paragraph.}
• line 9: wavenumber that indicates
• p.1521, line 2: {'certain': what do you mean by 'certain universality? As opposed to uncertain? If so, why are you certain? If not, do you mean certain as in synonymous with 'specific'? If so, be specific and explain which universality it is}
• line 4: is in a reasonable agreement

Response: All typos are corrected as suggested by the referee.

J. D. Tellez Alvarez
jackson.david.tellez@upc.edu

The interest of this paper in using laboratory experiments to model geophysical complex flows is dual: Besides confirming the role of Coriolis beta effect on the latitudinal range of vortex sizes, the presentation and use of AIV (Altimetric Imaging Velocimetry) may be used both in the laboratory and in Geophysical and Environmental field and satellite analysis.
The technique of applying PIV like spatial and temporal correlation analysis on the Gradients of measured height and presenting its spectra provides very interesting turbulence information in order to examine the rotating stratified flows.

It would be interesting to detail more the way in which the gradient vector field is presented it the plots as a scalar, and what is the range of precision in determining actual heights.

Response: The velocity gradient is represented by color (which can be considered as 2-parameter space). Please see more details of the method in Afanasyev et.al., Exp Fluids 2009

How the Spectra of the height variation of the flow relates to actual Lagrangian Tracer Spectra is assumed from a barotropic behavior of the flow, can you detect any actual baroclinic mixing events and local vorticity production ?

Response: The QG velocity field should be close to one obtained from Lagrangian Tracers if the Rossby number is not too large. It is the case here.

Some specific comments and questions:

1,- in the page 1510 – line 10: you have a concentration of salt 30 ppt, in the brine, why do you decide this kind of concentration, Was the reason to mach the concentration of salt, so the buoyancy was comparable to that due to the heat flux and the thermal gradient experiments?. It would be important to present the Richardson numbers or the buoyancy fluxes for both types of experiments.

Response: We actually did a series of experiment with different salinity difference. They are qualitatively similar and we chose this particular one to discuss spectra in this paper.

2,- page 1511 – line 5. From your comments: Do you think this technique, not only can be extrapolated to determine the vortices in oceanografic context, maybe if can also possible to calculate the vortex induced deformations of the surface in some river estuaries, or in some areas where the river outflow mixes with the ocean salty water. Or in the situation of the Mediterranean outflow in the Atlantic (Meddies)

Response: Altimetry is of course widely used in oceanography. It is all about the sufficient resolution of the data and the applicability of the QG approximation (for velocity calculation).

3,- in page 1512: Because you comment that the velocity was calculate using a (quasi-) geostrophic approximation, which is an indirect method, did you check this method with independent measurements, or have you considered the possibility to generate an alternative field of velocity with direct PIV or with the dispersive characteristic velocity obtained with some floating tracers.

Response: Yes, we did. Please see Afanasyev et.al., Exp Fluids 2009.

4,- From Figure 1: what is the heigh of the camera position in the experiments, and if the position of the camera is vertical. How do you avoid the errors due to the video parallaxing, and how does the rotation affect the sides and centre of the tank, because you have both the slope of the surface flow and the slope (parabolic) of the (salt or heat) interface?

Response: Parabola is not very steep here. We don't correct for camera parallax because the camera lens is quite good. But it can be done, of course, if need to be.

5,- Figures 4 and 5 showing the spectra of both heat and salt experiments should have the same axes so comparisons are better made

6,-Can you estimate the pdf of vortices (heigh structures) as a function of (Latitude) radial position within the tank, It is clear that vortices near the (Pole) centre are smaller than near the (Equator) sides of the tank. In both experiments plots will be different (as Spectra are also) but could it be possible to collapse the data with a suitable length scale ?

Response: This is a good suggestion, we will look into it and report elsewhere.

Complex environmental beta-plane turbulence: Laboratory Experiments with Altimetric Imaging Velocimetry

A. M. Matulka[1], Y. Zhang[1], and Y. D. Afanasyev[1]

[1]{Memorial University of Newfoundland, St. John's, Canada}

Correspondence to: Y. D. Afanasyev (afanai@mun.ca)

Abstract

Results from the spectral analyses of the flows in two experiments where turbulent flows were generated in a rotating tank with topographic β-effect, are presented. The flows were forced either by heating water from below or supplying fresh water at the top of a saline layer. The flow was essentially barotropic in the first experiment and baroclinic in the second experiment. The gradient of the surface elevation was measured using optical altimetry (Altimetric Imaging Velocimetry). Multiple zonal jets of alternating direction were observed in both experiments. Turbulent cascades of energy exhibit certain universal properties in spite of the different nature of flows in the experiments.

1 Introduction

Two-dimensional β-plane turbulence is an important concept in complex environmental flows where planetary rotation and the effect of the variation of the Coriolis parameter with latitude (β-effect) are significant factors. Kraichnan (1967) formulated a Kolmogorov-type theory which predicted the slope -5/3 of the energy spectrum in the energy range and the slope -3 in the enstrophy range for two-dimensional turbulence. The β-effect modifies two-dimensional turbulence towards anisotropy. The energy spectra in wavenumber space become a figure-of-eight with most of the energy concentrated at zonal wavenumber close to zero. In physical space this effect manifests itself in the creation of zonal jets. Oceanographic observations of this phenomenon have been extensively discussed in the literature (Maximenko et al., 2005, 2008; Centurioni at al., 2008; Ivanov et al. (2009)).

Experiments on the Coriolis rotating platform by Read et al. (2007) confirmed the theoretical prediction of -5/3 slope in the energy range. The authors used convective forcing in their experiments which generated motions of very small scale. Since the size of the domain was large, the scale separation was large enough for the development of the inverse cascade of energy. A recent study on two-dimensional turbulence (in the absence of β-effect) by Afanasyev and Craig (2013) gave the experimental evidence of dual cascade with the spectral slopes of -5/3 and -3. Further experiments with barotropic turbulence on the β-plane by Zhang and Afanasyev (2014) demonstrated the dual cascade in the presence of β-effect as well as a “figure eight” energy spectrum in the wavenumber space.

Zonal jets have a long history of investigation starting from the pioneering experiments by Whitehead (1975) and Colin de Verdiere (1979). The jets readily form when a spatially localized forcing is applied in the β-plane fluid (e.g. Sommeria et al., 1988, 1989; Marcus and Lee, 1998, Afanasyev et al., 2011, 2012; Slavin and Afanasyev, 2012). However, a distributed forcing such as that provided by baroclinic instability, also creates jets. In the ocean, the regions where baroclinic instability is dynamically important include the Antarctic Circumpolar Current (ACC) as well as western boundary currents and their extensions. Multiple jets as well as mesoscale eddies are created there by the baroclinic instability thus forming a dynamically complex turbulent flow. A classic model for a baroclinically unstable system is a rotating annulus where heating/cooling is provided at the outer wall/center of the tank respectively. Different aspects of the dynamics of this system were studied in a number of experiments (Hide and Mason, 1975; Mason, 1975; Bastin and Read, 1997, 1998; Wordsworth et al., 2008; Smith et al., 2014). A somewhat different experimental approach to modelling a baroclinically unstable two-layer flow with vertical shear was used in a recent study by Matulka and Afanasyev (2015). It was shown that the meridional scale of the jets is determined to large extent by the radius of deformation and, at the same time, is in good agreement with the Rhines scale (Rhines, 1975). The jets are driven by (nonlinear) Reynolds stresses due to baroclinic meanders. This is in agreement with a scenario described by Berloff et al. (2009 a, 2009 b). The authors describe the formation of jets as a secondary instability of the primary instability of the baroclinic flow in the form of mainly meridional motions (so-called "noodles").

In this study we perform spectral analyses of the flows described in Matulka and Afanasyev (2015) and compare them with the results obtained for a somewhat different flow generated by thermal forcing (Zhang and Afanasyev, 2014). The latter experiment although forced baroclinically was more barotropic in its dynamics while the former experiment was purely baroclinic. In Sec. II of this paper, we describe the laboratory setup for both experiments. In Sec. III the results of the spectral analyses are reported. Concluding remarks are given in Sec. IV.

2 Experimental technique

The laboratory experiments were carried out in a cylindrical tank of radius R = 55 cm filled with water of depth H_0 = 10 – 12 cm. The tank was installed on a rotating table (Fig. 1 a) and rotated in an anticlockwise direction at a constant angular rate Ω = 2.32 rad/s. In this paper we compare two experiments where the flows were forced in two different ways. The first experiment was forced thermally with a heating wire at the bottom of the tank. The wire was arranged in an approximately uniform pattern such that the distance between the segments of the wire was 4.5 cm. Figure 1 b shows the magnitude of velocity in the range between 0 (black) and 0.5 cm/s (white) in the very beginning of the experiment. The flow is initially along the wires such that the wire pattern is visible. This wire arrangement (in contrast to, say, a spiral) was chosen in order to avoid a direct forcing in the zonal direction but yet to provide an appoximately uniform mean heat flux across the bottom. The heater supplied the total power of 2300 W.

In the second experiment the flow was forced by delivering fresh water at the surface of a salt water layer of salinity S = 30 ppt. The fresh water source was distributed along the wall of the tank and created a coastal current flowing counterclockwise around the tank. The fresh water was pumped into the tank by a pump which delivered 20 liters of water in about 6 min. Figure 1 c shows the camera view of the flow in the middle of the forcing period when the fresh water from the source has not yet spread over the entire surface of the tank but is concentrated mainly in the coastal current.

The free surface of the rotating fluid is a paraboloid when in solid-body rotation. The height of water surface varies quadratically with the distance r from the axis of rotation

$$h(r) = H_0 + \frac{\Omega^2}{2g}\left(r^2 - \frac{R^2}{2}\right) \qquad (1)$$

where g is the gravitational acceleration. This creates a topographic (polar) β-plane where the β-parameter at some distance $r = r_0$ from the pole is given by

$$\beta = \frac{f_0}{h(r)} \left.\frac{dh(r)}{dr}\right|_{r=r_0} \qquad (2)$$

where f_0 = 2Ω is the Coriolis parameter. The values of the β-parameter in our experiments were between 0.07 and 0.1 $cm^{-1}s^{-1}$.

We use the Altimetric Imaging Velocimetry (AIV) system to measure the gradient of the surface elevation η (for more details see Afanasyev et al. 2009). AIV is based on optical altimetry first described in Rhines et al. (2006). Laboratory altimetry is not unlike the satellite altimetry which became an irreplaceable tool in oceanography. Apart from measuring $\nabla\eta$, AIV can be used as a tool to visualize the entire surface of the rotating fluid just like satellite altimetry provides a global coverage of the Earth's oceans. The AIV also provides an alternative to a well-known Particle Imaging Velocimetry (PIV) technique. To obtain the velocity field using PIV one has to find correlations between small areas (typically 12 – 48 pixels in both dimensions) of two successive images of the flow. If a camera has an imaging array of size say 1000×1000 pixels, the resulting array of velocity vectors has dimensions less than 100×100. Thus, the PIV technique effectively reduces the spatial resolution by a factor of 100 or more. AIV, on the other hand, allows one to obtain the velocity vector in every pixel of the image, which makes its spatial resolution practically unlimited given that the cameras with large imaging arrays are now easily available. The limitation of the AIV is that it can only be used in a relatively fast rotating fluid with free surface. It is, however, perfectly suited for oceanographic fluid dynamics experiments on the β-plane as those described in this paper. Paraboloidal surface of the rotating fluid is used like the mirror of a Newtonian telescope. If the surface is disturbed by the pressure perturbations due to the flow, the slope of the surface changes slightly. These perturbations of the slope are detected by the AIV and measured using simple geometry and a color coding.

AIV measures an "exact" (within experimental accuracy) surface elevation gradient, $\nabla\eta$, which translates into the pressure gradient, $\nabla p = \rho g \nabla\eta$, at the surface. Note that the main uncertainty is due to the color noise of the camera sensor. To reduce the noise we pass data through a median filter with a window size of 5×5 pixels (physical size of approximately

0.2×0.2 cm). The overall uncertainty of $\nabla \eta$ can be estimated to be approximately 5%. The velocity field is not measured directly by the AIV but rather obtained from the measured $\nabla \eta$ using a (quasi-) geostrophic approximation.

The barotropic component of velocity can be calculated in geostrophic approximation as follows

$$\mathbf{V} = \frac{g}{f_0}\left(\mathbf{n} \times \nabla \eta\right), \tag{3}$$

where is **n** is the vertical unit vector. A next order of approximation is provided by the quasi-geostrophy which gives

$$\mathbf{V} = \frac{g}{f_0}\left(\mathbf{n} \times \nabla \eta\right) - \frac{g}{f_0^2}\frac{\partial}{\partial t}\nabla \eta - \frac{g^2}{f_0^3} J\left(\eta, \nabla \eta\right), \tag{4}$$

where *J* is the Jacobian operator. The second and the third terms in the RHS of Eq. (4) are corrections to the geostrophic velocity which take into account transient and nonlinear effects. Their relative importance is determined by the temporal Rossby number $Ro_T = 1/(f_0 T)$ and the Rossby number $Ro = U/(f_0 L)$ respectively. Here *T* is the time scale of the unsteady processes in the flow, while *U* and *L* are velocity and length scales of the flow. Thus, the velocity field is determined more accurately when the flow is closer to being quasigeostrophic. “Textbook” theory on the validity of the quasigeostrophic approximation applies here. Since the Rossby number did not exceed unity even in the core of the eddies in our experiments and the mean values of the Rossby number were of the order of 10^{-1}, the velocity was, on average, within 10% of the “exact” velocity.

Relative vorticity, $\zeta = \mathbf{n} \cdot curl\mathbf{V}$, was calculated by differentiating the velocity field. Since numerical differentiation amplifies noise in the original data, we used the Sobel gradient operators with 5 × 5 kernels (e.g. Pratt, 2007). The kernels are convolved with the velocity data to calculate the derivatives in x- and y-directions.

According to the Taylor-Proudman theorem, the surface velocity given by Eq. (4) is a good approximation for the velocity in the entire column of water except the Ekman layer at the bottom. Note that in a stratified fluid, as in our two-layer experiment with saline forcing, the velocity field obtained by altimetry is, in fact the barotropic component of the total velocity in the entire layer of water. It is also the upper layer velocity. A baroclinic component which allows one to obtain the total velocity in the lower layer can be measured by a different technique (e.g. Afanasyev et al., 2009; Matulka and Afanasyev, 2015) but is not discussed here.

3 Results

We performed two sets of experiments with different forcing, namely the thermal forcing by a wire-heater at the bottom and the saline forcing by injection of fresh water at the wall. In what follows we discuss them in parallel highlighting the similarities and differences between them.

3.1 General flow evolution

Figure 2 a shows a typical snapshot of the surface of water in the experiment with the thermal forcing when the flow is fully developed. The flow is visualized by the AIV technique such that color shows the horizontal gradient of the surface elevation, $\nabla\eta$. The colour intensity indicates the magnitude of $\nabla\eta$ while hue shows its direction. The motions are initially of very small scale in this experiment (see also Fig. 1 b). Warm water heated by the wire rises to the surface in thin sheets and forms long thin filaments. These filaments are unstable with respect to baroclinic or frontal instability and break into small eddies. The size of the eddies is most likely determined by the baroclinic radius of deformation which can be defined as $R_d = \left(g' H_0/2\right)^{1/2} \big/ f_0$, where g' is the reduced gravity in the warm water filaments and eddies. The reduced gravity is defined by the temperature difference between the water in filaments and background temperature of the water in the tank. However, since we did not measure the temperature field in this experiment, we cannot pinpoint the exact value of R_d. It is important to establish here the values of control parameters for the thermal convection in this experiment. Flows created by buoyancy sources in the rotating fluid (in the absence of the β-effect) were studied in laboratory experiments by Fernando et al. (1991) and Maxworthy and Narimusa (1994). The energy flux per unit area of the bottom of the tank is Q = 2.5 $\times 10^3$ Wm^{-2} in our experiments. This translates into the buoyancy flux $B = \alpha g Q/C_\mathrm{p}$ = 1.2 $\times 10^{-6}$ m^{2}s^{-3}, where α is the thermal expansion coefficient and C_p is the volumetric heat capacity of water at constant pressure. A dimensionless parameter which controls the regime of the thermal convection is the Rayleigh number. The flux Rayleigh number is quite high in our experiments, $Ra_{flux} = BH_0^4 / \nu^2\kappa$ = 1.8×10^9 (where κ is the thermal diffusivity of water) that indicates a regime of turbulent convection. Comparing to the recent experiments by Read et al. (2015) where similar heating was used but in an experiment of a larger scale, we note that our buoyancy flux was almost two orders of magnitude higher; the Rayleigh number was, however, an order of magnitude lower because of the smaller depth of water in our experiments.

Figure 3 a, b shows the fields obtained as a result of the velocity calculation from measured $\nabla\eta$ in the thermal experiment. Azimuthal velocity, V_{az} in a polar coordinate system with the origin at the center of the tank is shown in panel a, while panel b shows the relative vorticity, $\zeta = \mathbf{n} \cdot curl\mathbf{V}$. The relative vorticity field shows a fine structure of the flow with multiple small scale cyclonic (red) and anticyclonic (blue) eddies. The relative vorticity is normalized by the Coriolis parameter f_0 , thus the image in panel b can be interpreted as a map of the Rossby number, Ro = ζ/f_0 . The values of Ro can reach unity in the strongest eddies while the rms value is approximately 0.2. An original alignment of filaments with the heating wires can still be seen in the central area of the tank while closer to the wall where the water is deeper and the β-effect is stronger, the bands of positive and negative vorticity are aligned in the zonal direction which indicates the presence of zonal jets. The jets can be seen more clearly in the azimuthal velocity image in panel a. The circulation is mainly in the counterclockwise (eastward) direction (V_{az} is positive, red color). Maximum values of V_{az} in the jets are approximately 1 cm/s.

Figure 2 b and Figure 3 c, d (see also Fig. 1 c) show the experiment with the saline forcing. The water in the tank is initially of salinity $S = 30$ ppt. When a source distributed along the wall of the tank delivers fresh water, it creates a current along the wall. This current is initially wedge-shaped in cross-section and is approximately in geostrophic balance such that it „leans" on the wall to its right. This coastal current can be seen clearly in Figures 1 c, 2 b and 3 c, the velocity of the current is initially in excess of 5 cm/s. The current is baroclinically unstable (e.g. Griffiths and Linden, 1981) and creates meanders which penetrate into the interior of the tank. During the forcing period of the experiment when the source continuously supplies fresh water, the entire surface of the tank eventually becomes covered with a layer of fresh water. Thus, a two-layer system is created. The forcing then stops and the flow is allowed to develop freely. The depth of the upper layer is not uniform in the radial direction after the period of forcing. The layer is much thicker at the wall of the tank rather than at its center. Thus, the system contains a large amount of available potential energy which is released gradually and maintains the flow for a very long time after the forcing stops. The adjustment involves slow radial motion towards the center in the upper layer and the motion in the opposite direction in the lower layer. The radial motion, in turn, causes zonal circulation. Measurements of barotropic and baroclinic components of velocity (for details see Matulka and Afanasyev, 2015) show that the upper layer rotates cyclonically while the lower layer rotates anticyclonically. The shear between the layers makes the system baroclinically unstable. Conditions for the development of the baroclinic instability are maintained over a long period of adjustment. Note that measuremens of mean energy and enstrophy of the system (not shown here) during the long period of adjustment indicate that the system is approximately steady in this experiment.

Baroclinic instability together with other instabilities including, perhaps, wave breaking and barotropic and frontal instabilities, continuously generates meanders over the entire area of the tank. The meanders move water parcels in the radial (meridional) direction. According to conservation of potential vorticity the parcels aquire additional relative vorticity and radiate Rossby waves. Motion of the meanders/parcels correlated via the global Rossby wave field creates the Reynolds stresses which drive zonal jets in the interior of the tank. Thus, although direct forcing was stopped, the system is forced by the baroclinic instability similar to that in the ocean. Measurements of the Reynolds stresses in this experiment showed that jets in the interior are dynamically different from the coastal jet which is affected by the presence of the wall. The jets in the interior are true eddy-forced jets while the coastal current is not. In what follows we perform spectral analyses of the flow in the inner area which containes these “true“ jets and excludes the coastal current.

Visual comparison between the fields in the experiments with different forcing (Figure 3) shows that the scales of the turbulent eddies generated by the forcing are noticeably different. The eddies in the thermal experiment are smaller which indicates smaller R_d.

Another difference is perhaps more significant in distinguishing between the forcing mechanisms. The flow with saline forcing is characterised by thin filaments rather than circular eddies. In fact, eddies appear only as a result of breaking of the filaments and do not have very long lifetime. The filaments are created by the baroclinic instability; they protrude in the radial (meridional) direction. We hypothesise that these filaments are the manifestation of the so-called “noodles” which are the primary mode of the instability of the baroclinic flow (Berloff et al., 2009 a, 2009 b).

3.2 Energy spectra in wavenumber space

Herein we describe the results of the spectral analysis of the flows. For a circular domain such as our tank, it is perhaps more natural to use polar coordinates for the purpose of spectral decomposition. Afanasyev and Wells (2005) used Fourier-Bessel transform to obtain two-dimensional energy spectra of the polar β-plane turbulence in the space of azimuthal and radial wavenumbers and then to obtain one-dimensional spectrum by sorting data in terms of a polar analogue of the Cartesian isotropic wavenumber. However, it is easier to perform digital Fourier decomposition in the Cartesian coordinates because Fast Fourier Transform routines can be used. Moreover, usage of Cartesian coordinates and a conventional β-plane (rather than quadratic polar β-plane) simplifies the further comparison with available theory. For these reasons here we introduce a local Cartesian coordinates (x, y) centred at the reference radius r_0 = 25 cm such that x-axis is directed to the east, $x = r_0\theta$ (where θ is the polar angle) and y-axis is directed to the north, $y = r_0 - r$. For the spectral analyses we chose a domain of half width 17 cm centred at the reference radius r_0 = 25 cm such that the polar part of the tank, where β-plane approximation is inappropriate, and the wall area, where the coastal jet dominates, were excluded.

The AIV technique gives velocity field on a regular rectangular grid covering the entire area of the tank. The velocity vector field was interpolated onto the local Cartesian coordinate system and then projected to eastward and northward directions to obtain zonal and meridional velocity components. Discrete Fourier transform of these velocity components then gives velocity $\mathbf{u}\left(k_x,k_y\right)$ in the wavenumber space $\left(k_x,k_y\right)$. The two-dimensional energy spectrum is given by

$$E\left(k_x,k_y\right)=\frac{1}{2}\left|\mathbf{u}\left(k_x,k_y\right)\right|^2 . \qquad (4)$$

Figure 4 shows two-dimensional spectra in the experiments with thermal and saline forcing. The spectra are measured in the beginning of both experiments when the spectral signature of the forcing is still strong, and at a later stage, when the spectra reached certain “saturation” and the turbulent cascades are developed. The spectral properties of forcing or background turbulent flow can be inferred from the initial spectra. In the experiment with thermal forcing the eddies generated by thermal plumes are quite small; their scale can be estimated from the value of wavenumber $k \approx 2.5$ cm^{-1} (outer ring in Figure 4 a) to be approximately 2.5 cm. Here $k=\left(k_x^2+k_y^2\right)^{1/2}$ is the isotropic wavenumber. These eddies are initially concentrated along the heating wires. The separation of the heating wires (approximately 4.5 cm) determines a wavenumber $k \approx 1.4$ cm^{-1} where energy concentration is observed as well (inner ring in Figure 4 a). In the experiment with saline forcing the initial spectrum is determined by the baroclinic instability which is sustained in the two-layer system even when the actual forcing (the injection of fresh water) is stopped. The energy is distributed in a wide range of wavenumbers but is mainly contained within a circle which corresponds to the reciprocal of the radius of deformation, R_d^{-1}= 1.2 cm^{-1}. This is in agreement with the prediction of the Phillips model (Phillips 1951) of baroclinic instability.

The model predicts that all perturbations of wavenumber $k < R_d^{-1}$ are unstable with the most unstable (before nonlinear saturation) wavenumber being $k = 0.64\, R_d^{-1}$. Thus the initial spectra for both experiments confirm our initial observation that the forcing scale is smaller in the experiment with the thermal forcing. The spectra measured in much later times in both experiments (Figure 4 b, d) show that energy cascades towards smaller wavenumbers (larger scales). The distribution of energy in the wavenumber space also becomes more anisotropic; the energy flows towards the k_y axis (zonal modes, $k_x = 0$).

The inverse energy cascade is a well-known phenomenon in two-dimensional turbulence; energy is transferred from small scales (large k) to large scales (small k). In the presence of β-effect, this scenario is modified. The pioneering work by Rhines (1975) demonstrated that there is a certain scale, now known as the Rhines scale, which separates the large-scale motions where β-effect dominates from a small-scale turbulence. A wavenumber corresponding to the Rhines scale is given by

$$k_R = \sqrt{\beta / U_{rms}} \,, \qquad (5)$$

where U_{rms} is root-mean-square velocity. On large scales Rossby wave elasticity is important and the flow becomes strongly anisotropic as the (linear) dispersion relation for Rossby waves suggests. The anisotropy is manifested by the appearance of zonal jets. The wavenumber k_R is also widely used as an estimate for the meridional wavenumber of an arrangement of zonal jets. It was shown to work well in different circumstances including flows on gas giants or flows in the laboratory although different modifications of the Rhines scale were discussed as well. The values of k_R for each experiment are indicated by crosses on y-axis in Figure 4 b, d.

To extend the Rhines' argument to two dimensions one can equate the frequency of turbulent eddies to that of Rossby waves to obtain (Vallis and Maltrud, 1993) a dividing line in the form

$$k_8 = \sqrt{\frac{\beta \cos\theta}{U_{rms}}}, \qquad (6)$$

where θ is the polar angle in the wavenumber space, $\theta = \arctan(k_y / k_x)$. The line given by (6) resembles a figure-of-eight or a dumbbell and is shown in Figure 4 b, d. Note that values of U_{rms} are not given by theory but have to be measured in the experiment. Here we used the rms values of the y-component of velocity instead of the total velocity in order to avoid the mean flow in the azimuthal direction which occurred to different extent in both of the experiments. Since Rhines' theory assumes isotropic small-scale turbulence, it seems that the y-component of velocity represents a better measure of turbulence in our case. Spectra in Figure 4 b, d show that the turbulent cascade of energy due to nonlinear interaction of modes does not continue in the isotropic manner within the area bounded by k_8 line. In fact, there is little energy inside this area. The energy follows instead a (linear) Rossby wave dispersion relation flowing along the k_8 line towards the k_y axis and concentrating there. It is eventually dissipated by friction which in our case is mainly the Ekman bottom friction which acts on all scales. The distribution of zonal energy indicates that the isotropic Rhines scale is indeed a reasonable measure of the jet wavenumber in both experiments.

To study general spectral characteristics of the turbulent cascade without regard to the anisotropy one can average energy over the polar angle θ in the wavenumber space. As a result, one obtains a one-dimensional energy spectrum which is defined as $E(k) = 2\pi k \langle E(\mathbf{k}) \rangle$, where $\mathbf{k} = (k_x, k_y)$ and the average is over $|\mathbf{k}| = k$. Figure 5 shows the one-dimensional spectra for our two experiments. Theory of two-dimensional turbulence without β-effect predicts the existence of the dual cascade such that energy cascades to large scales in the range $k < k_F$ with a Kolmogorov type spectral slope -5/3 and to small scales in the range $k > k_F$ with a slope -3. Here k_F is the forcing wavenumber where energy is injected into the system. The former range is called the energy range while the latter is called the enstrophy range. The forcing wavenumber can be estimated to be $k_F \approx 2.5$ cm^{-1} in the experiment with thermal forcing and $k_F = 0.64 R_d^{-1} \approx 0.8$ cm^{-1} in the experiment with saline forcing. These values mark the boundary between the energy and enstrophy ranges in both experiments. Figure 5 shows that the spectral slope does change in the vicinity of the estimated forcing wavenumbers that confirms that these estimates are meaningful. In both experiments, -5/3 slope was observed in the energy range; in the first experiment (thermal forcing) this range was longer than that in the second one (saline forcing). In the enstrophy range the -3 slope was observed in the first experiment (thermal forcing) while the second experiment (saline forcing) showed a much steeper slope. The presence of the -3 slope might be another consequence of the mostly barotropic (and two-dimensional) character of the flow in the first experiment. Indeed, the flow in this experiment is convectively unstable and mixing is significant. As a result, the fluid is not significantly stratified and the flow must be mainly barotropic. The steeper slope in the second experiment is, perhaps, due to the fact that this two-layer, statically stable flow is significantly baroclinic. Note that steeper than -3 slope was also measured in the experiments with shallow water, f-plane turbulence by Afanasyev and Craig (2013) and in the numerical simulations by Yuan and Hamilton (1994).

The estimates of the Rhines wavenumber (accidently) give similar values for both experiments, $k_R \approx 0.45$ cm^{-1}. This value indicates the place for zonal jets in the spectral cascade. The maximum energy achieved by the cascade in the second experiment roughly corresponds to the Rhines wavenumber which indicates that zonal motions should possess a significant portion of the total energy. In the first experiment, the cascade does not quite reach the Rhines wavenumber. Note that the Rhines wavenumber does not stop the cascade to even lower wavenumbers; the cascade is just redirected towards zonal motions.

4 Conclusions

In our experiments we observed the formation of zonal jets in the experiments where flows were forced using two different methods. Perhaps the main difference between the forcing was that the heater at the bottom created convectively unstable vertical temperature distribution which resulted in small scale convective plumes. Vertical mixing must be significant in this system and the fluid remained mainly unstratified. The large scale flow in this experiment is then approximately barotropic, although the nature of forcing is baroclinic. In the second experiment, on the other hand, we created statically stable two-layer stratification. The flow was baroclinic to a significant degree. Since this system was unstable with respect to baroclinic instability, the instability as a source of small-scale turbulence. Thus in both cases some small-scale turbulence was created but in the former experiment the flow was mainly barotropic while in the latter it was mainly baroclinic.

In spite of this significant difference between the flows in our two experiments, we observed a definite universality in their spectral dynamics. The energy cascaded from small scales to larger scales and towards zonal motions. The two-dimensional spectra demonstrated that this cascade is in reasonable agreement with the Rhines theory. One-dimensional spectra of energy reliably demonstrated the existence of the energy interval with the -5/3 slope. Note that although in our experiments one can infer the direction of the energy cascade from the form of the spectrum assuming that the forcing wavenumber is known, direct evidence of the cascade direction can only be provided by the analyses of the spectral energy flux. Such evidence was provided for shallow water rotating turbulnce (without β-effect) in the laboratory investigation by Afanasyev and Craig (2013) The analysis of the energy flux for the large-scale oceanic turbulence by Scott and Wang (2005) revealed the existence of the inverse cascade in agreement with the two-dimensional turbulence theory. However, the interplay between barotropic and baroclinic modes and the extent each mode contributes to the cascade in the ocean still remains a subject of research. The analysis of the flux for the experiments reported here is yet to be done and will be reported elsewhere.

Acknowledgements

The authors are grateful to Alexander Slavin for his help with one of the experiments. YDA is supported by the Natural Sciences and Engineering Research Council of Canada. Experimental data are available on request from Y. D. Afanasyev.

References

Afanasyev, Y. D., and Craig, J. D. C.: Rotating shallow water turbulence: experiments with altimetry, Phys. Fluids, 25, 106603, doi:10.1063/1.4826477, 2013.

Afanasyev, Y. D., O'Leary, S., Rhines, P. B., and Lindahl, E. G.: On the origin of jets in the ocean, Geoph. Astroph. Fluid Dyn., 106 (2), 113, 2011.

Afanasyev, Y. D., Rhines, P. B., and Lindahl, E. G.: Velocity and potential vorticity fields measured by altimetric imaging velocimetry in the rotating fluid, Exp. Fluids, **47**, 913, 2009.

Bastin, M.E., and Read, P. L.: A laboratory study of baroclinic waves and turbulence in an internally heated rotating fluid annulus with sloping endwalls. J. Fluid Mech., 339, 173–198, 1997.

Bastin, M. E., and Read, P. L.: Experiments on the structure of baroclinic waves and zonal jets in an internally heated rotating cylinder of fluid. Phys. Fluids, 10, 374–389, 1998.

Berloff, P., Kamenkovich, I., and Pedlosky, J.: A model of multiple zonal jets in the oceans: dynamical and kinematical analysis, J. Phys. Oceanogr., 39, 2711–2734, 2009a.

Berloff, P., Kamenkovich, I., and Pedlosky, J.: A mechanism of formation of multiple zonal jets in the oceans, J. Fluid Mech., 628, 395–425, 2009b.

Centurioni, L. R., Ohlmann, J. C., and Niiler, P. P.: Permanent meanders in the California Current System, Phys. Oceanography, 38, 1690, 2008.

Collin de Verdiere, A.: Mean flow generation by topographic Rossby waves, J. Fluid Mech., 94, 39-64, 1979.

Fernando, H. J. S., Chen, R. R., and Boyer, D. L.: Effects of rotation on convective turbulence. J. Fluid Mech., 228, 513, 1991.

Griffiths, R. W., and Linden, P. F.: The stability of buoyancy-driven coastal currents. Dyn. Atmos. Oceans, 5, 281-306, 1981.

Hide, R., and Mason, P. J.: Sloping convection in a rotating fluid. Adv. in Phys., 24, 47–99, 1975.

Ivanov, L. M., Collins, C. A., and Margolina, T. M.: System of quasi-zonal jets off California revealed from satellite altimetry, Geoph. Res. Lett, 36, L03609, doi:10.1029/2008GL036327, 2009.

Kraichnan, R.: Intertial ranges in two-dimensional turbulence, Phys. Fluids, 10, 1417, 1967.

Marcus, P. S., and Lee, C.: A model for eastward jets in laboratory experiments and planetary atmospheres, Phys. Fluids, 10, 1474, 1998.

Mason, P. J.: Baroclinic waves in a container with sloping endwalls. Phil. Trans R. Soc. Lond., A278, 397–445, 1975.

Matulka, A. M., and Afanasyev, Y. D.: Zonal jets in equilibrating baroclinic instability on the polar beta-plane: experiments with altimetry, JGR-Oceans, 2015.

Maximenko, N. A., Bang, B., and Sasaki, H.: Observational evidence of alternating zonal jets in the world ocean, Geoph. Res. Lett., 32, L12607, doi:10.1029/2005GL022728, 2005.

Maximenko, N. A., Melnichenko, O. V., Niiler, P. P., and Sasaki, H.: Stationary mesoscale jet-like features in the ocean, Geoph. Res. Lett., 35, L08603, doi:10.1029/2008GL033267, 2008.

Maxworthy, T., and Narimousa, S.: Unsteady, turbulent convection into a homogeneous, rotating fluid, with oceanographic applications. J. Phys. Oceanogr., 24, 865-887, 1994.

Phillips, N. A.: A simple three-dimensional model for the study of large scale extra tropical flow pattern. J. Meteor., 8, 381–394, 1951.

Pratt, W. "Digital Image Processing", Wiley-Interscience, 2007.

Read, P. L., Yamazaki, Y. H., Lewis, S. R., Williams, P. D., Wordsworth, R., Miki-Yamazaki, K., Sommeria, J., Didelle, H., and Finchman, A.: Dynamics of convectively driven banded jets in the laboratory, J. Atmos Sci., 64, 4031, 2007.

Read, P. L., Jacoby, T. N. L., Rogberg, P. H. T., Wordsworth, R. D., Yamazaki, Y. H., Miki-Yamazaki, K., Young, R. M. B., Sommeria, J., Didelle, H., and Viboud, S.: An experimental study of multiple zonal jet formation in rotating, thermally driven convective flows on a topographic beta-plane. Phys. of Fluids, 27, 085111, doi: 10.1063/1.4928697, 2015.

Rhines, P. B.: Waves and turbulence on a beta-plane, J. Fluid Mech., 69(3), 417, 1975.

Rhines, P.B., Lindahl, E.G., Mendez, A.J.: Optical Altimetry: A new method for observing rotating fluids with application to Rossby waves on a polar beta-plane. J. Fluid Mech., 572: 389–412, 2006.

Scott, R.B., Wang, F.: Direct Evidence of an Oceanic Inverse Kinetic Energy Cascade from Satellite Altimetry. J. Phys. Oceanogr., **35**, 1650–1666, 2005.
doi: http://dx.doi.org/10.1175/JPO2771.1

Slavin, A. G, and Afanasyev Y. D.: Multiple zonal jets on the polar beta plane, Phys. A. Fluids, 24, 016603, doi:10.1063/1.3678017, 2012.

Smith, C. A., Speer, K. G., and Griffiths, R. W.: Multiple zonal jets in a differentially heated rotating annulus, J. Phys. Oceanogr., 44, 2273–2291, 2014.

Sommeria, J., Meyers, S. D., and Swinney, H. L.: Laboratory simulation of Jupiter's great red spot, Nature, 331, 689, 1988.

Sommeria, J., Meyers, S. D., and Swinney, H. L.: Laboratory model of a planetary eastward jet, Nature, 337, 58, 1989.

Vallis, G. K., amd Maltrud, M. E.: Generation of mean flows and jets on beta plane and over topography, J. Phys. Ocean, 23, 1351, 1993.

Whitehead, J. A.: Mean flow driven by circulation on a β-plane, Tellus, 27, 358, 1975.

Wordsworth, R. D., Read, P. L., and Yamazaki, Y. H. 2008. Turbulence, waves and jets in a differentially heated rotating annulus experiment. Phys. Fluids, 20, 126602, doi: 10.1063/1.2990042.

Yamazaki, K., Young, R. M. B., Sommeria, J., Didelle, H., and Viboud, S.: An experimental study of multiple zonal jet formation in rotating, thermally driven convective flows on a topographic beta-plane, Phys. Fluids, 27, 085111, doi:10.1063/1.4928697, 2015.

Yuan, L., and Hamilton, K.: Equilibrium dynamics in a forced-dissipative f-plane shallow water system, J. Fluid Mech., 280, 369, 1994.

Zhang, Y., and Afanasyev, Y. D.: Beta-plane turbulence: Experiments with altimetry, Phys. of Fluids, 26, 026602, doi:10.1063/1.4864339, 2014.

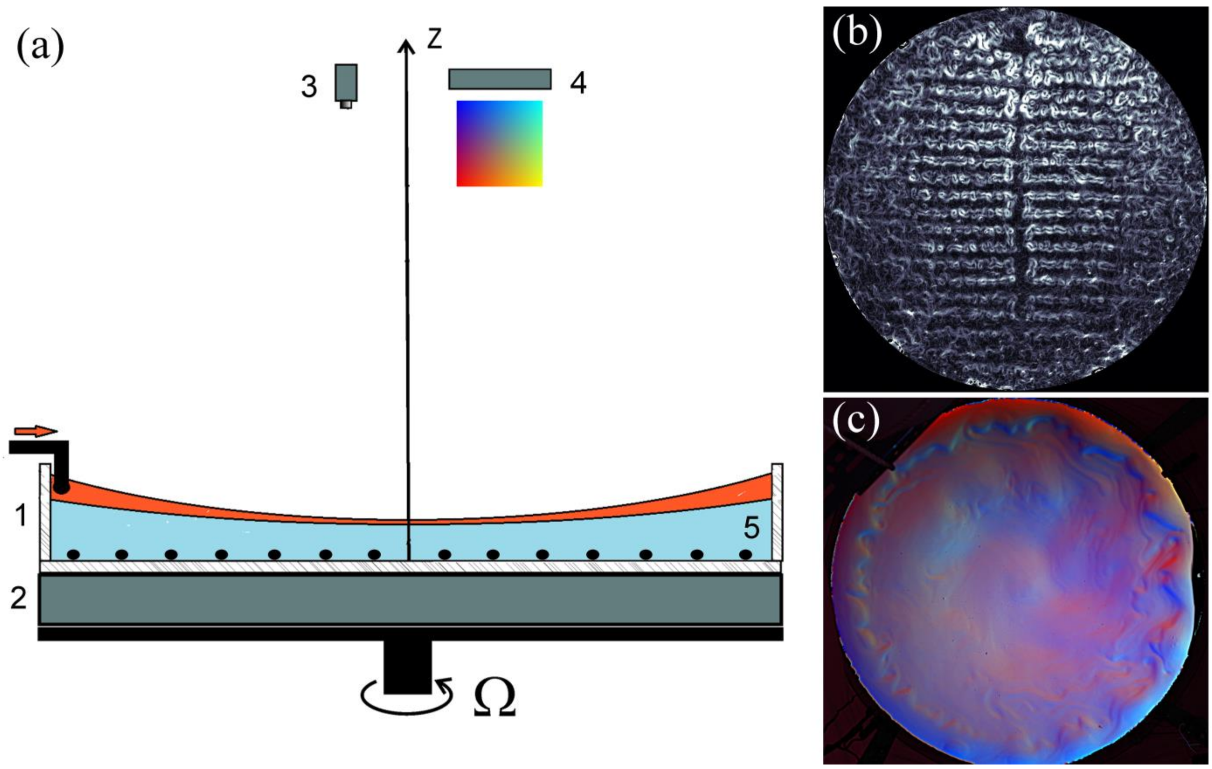

Figure 1. Sketch of the experimental setup (a) and view of the flow in the beginning of the experiments with the thermal (b) and saline (c) forcing: (1) cylindrical tank filled with water and installed on a table rotating with angular velocity Ω; (2) light box for the optical thickness measurements; (3) video camera; (4) light source with color mask; and (5) heating wire on the bottom.

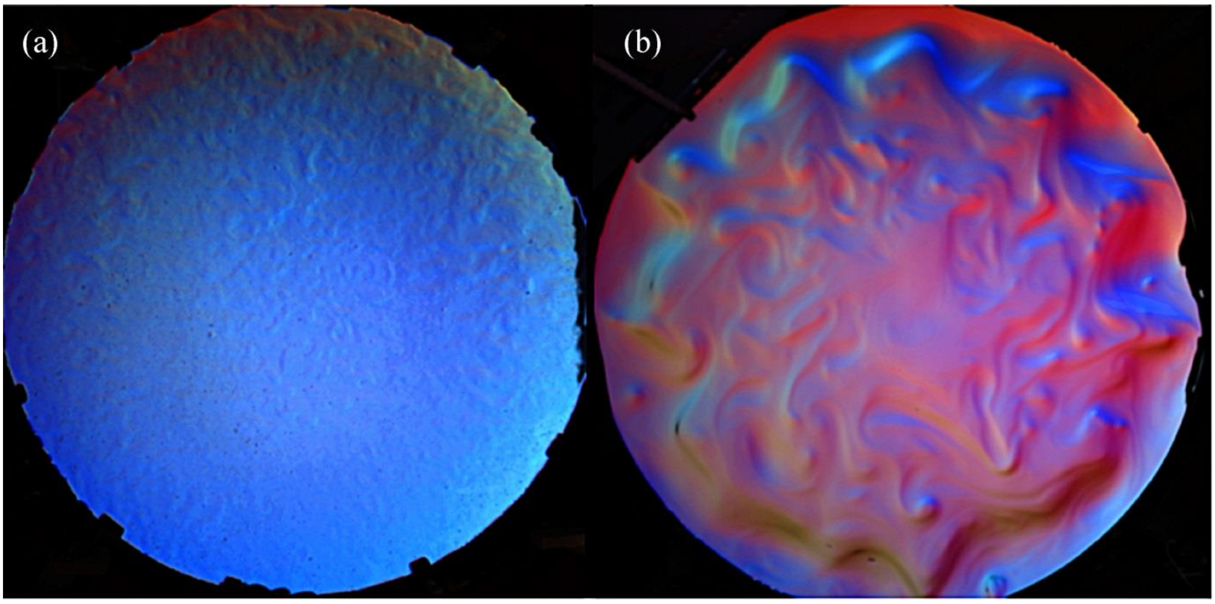

Figure 2. Typical images from video sequences recorded in the experiments with thermal (a) and saline (b) forcing. The flows are visualized by optical altimetry (AIV); different colors indicate different values (both in magnitude and direction) of the gradient of the surface elevation.

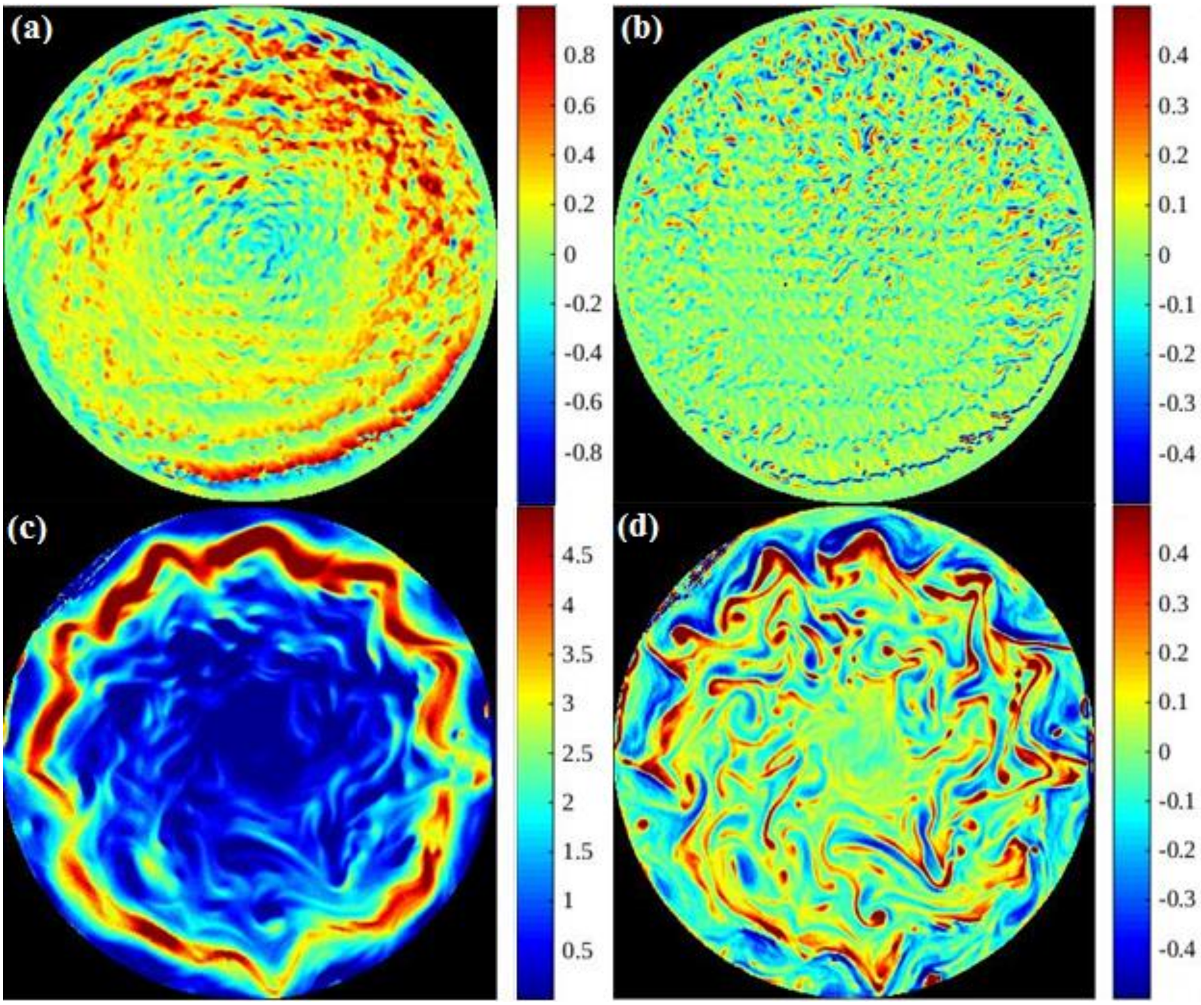

Figure 3. Flows generated by thermal forcing at t =280 s (a, b) and by saline forcing at t = 150 s (c, d). Panels (a) and (c) show the x-component of velocity (azimuthal velocity) u while panels (b) and (d) show the dimensionless relative vorticity, ζ / f_o. Salinity difference between the layers for the experiment with saline forcing (a, b) is S = 30 ppt. The center of the tank corresponds to the North Pole of the polar β-plane.

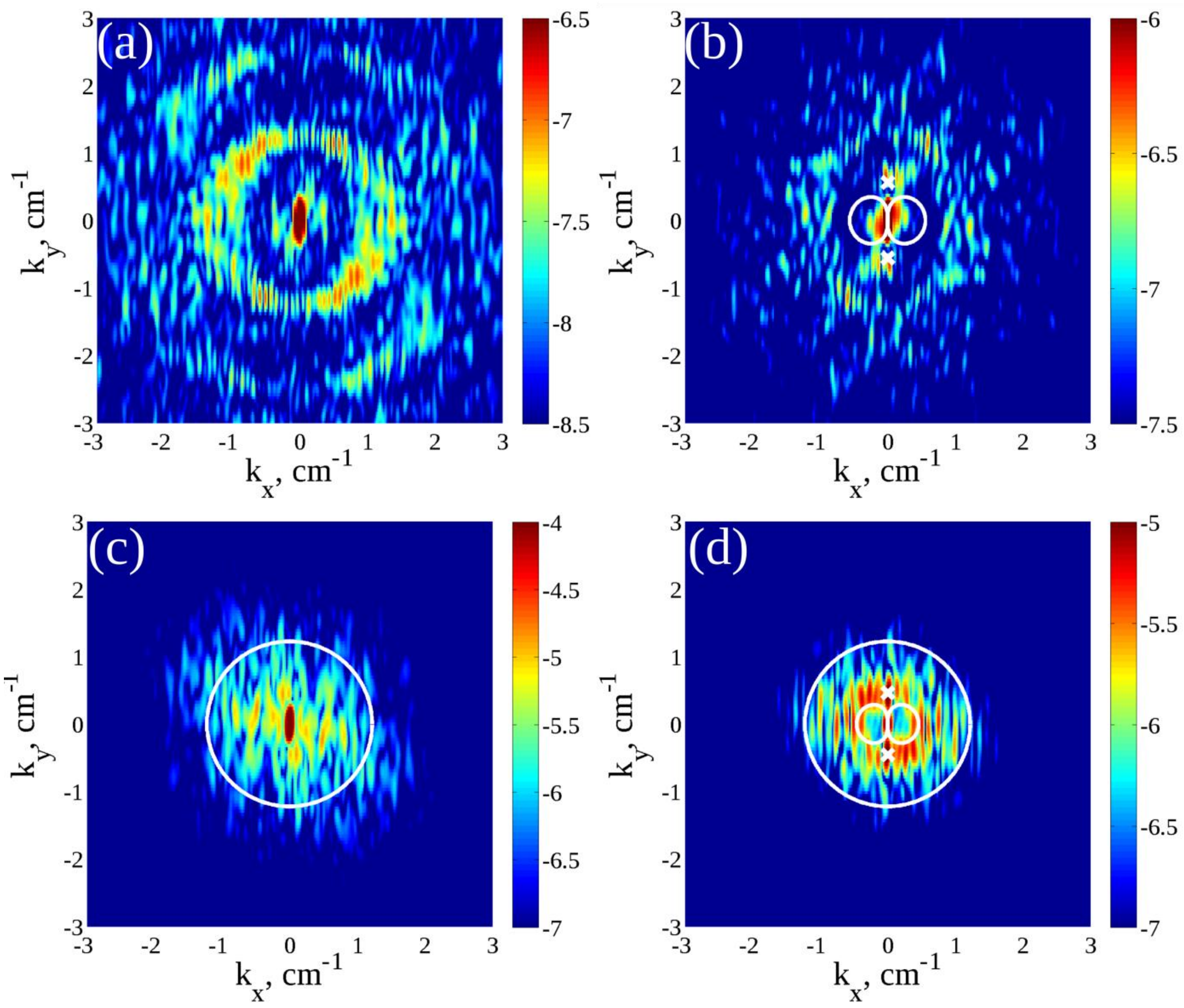

Figure 4. Energy spectra in the wavenumber space ($k_{x,}$ k_y) for the experiments with thermal (a, b) and saline (c, d) forcing: t = 30 s (a) 630 s (b) from the beginning of the thermal experiment; t = 10 s (c) 722 s (d) after the fresh water source stopped in the experiment with saline forcing. Color shows energy in logarithmic scale. Black circles in (c) and (d) show R_d^{-1}. Black crosses in (b) and (d) represent the Rhines scale wavenumber (5) while the dumbbell-shaped curve is given by Eq. (6).

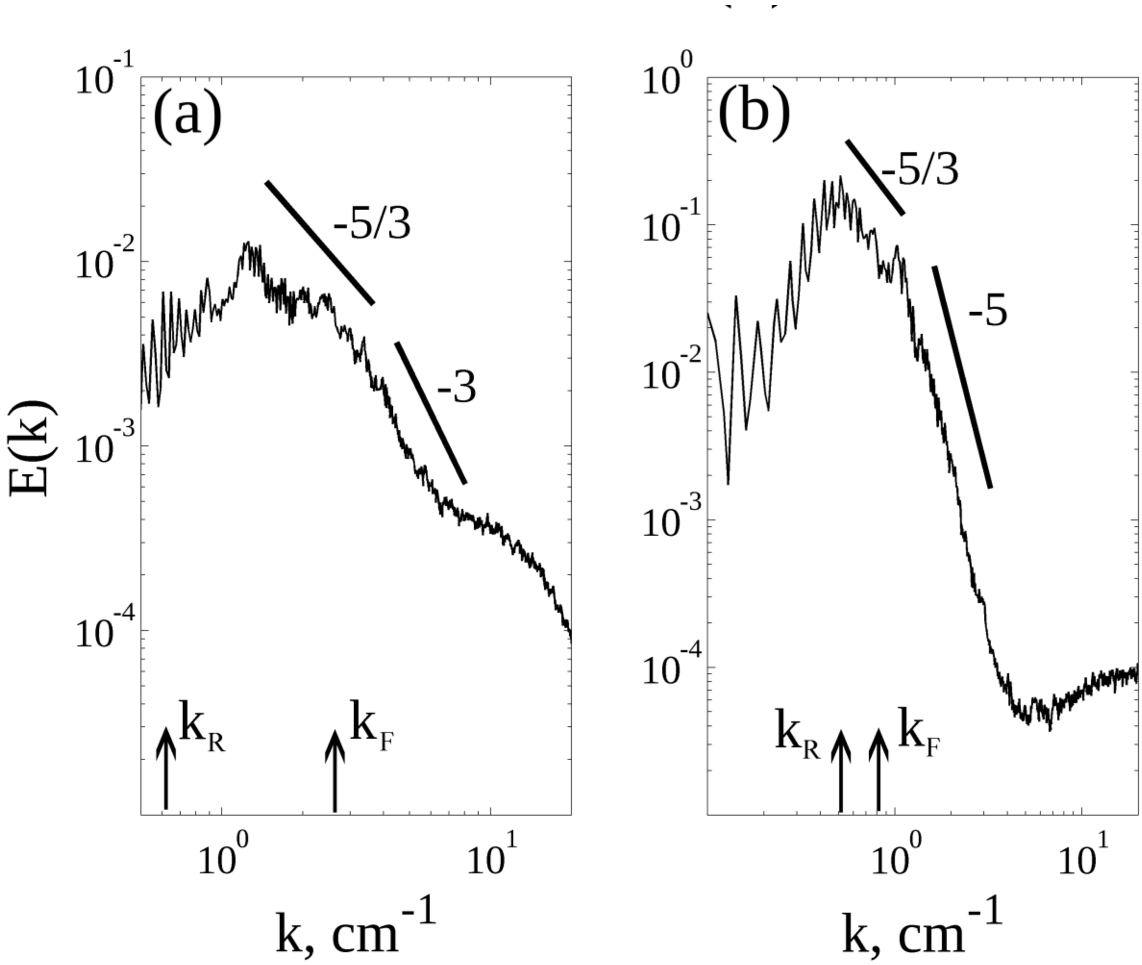

Figure 5. The one-dimensional energy spectra in log-log scale for the experiments with thermal (a) and saline (b) forcing: t = 630 s (a) 722 s (b) (as in Fig. 4 (b, d)).